Mon. Not. R. Astron. Soc. **396,** 668–679 (2009) doi:10.1111/j.1365-2966.2009.14746.x

Lensed CMB temperature and polarization maps from the Millennium Simulation

Carmelita Carbone,[1⋆] Carlo Baccigalupi,[2,3⋆] Matthias Bartelmann,[4⋆] Sabino Matarrese[5,6⋆] and Volker Springel[7⋆]

[1]*Institut de Ciències de l'Espai, CSIC/IEEC, Campus UAB, F. de Ciències, Torre C5 par-2, Barcelona 08193, Spain*
[2]*SISSA/ISAS, Astrophysics Sector, Via Beirut 4, I-34014, Trieste, Italy*
[3]*INFN, Sezione di Trieste, Via Valerio, 2, 34127, Trieste, Italy*
[4]*Institut für Theoretische Astrophysik, Universität Heidelberg, Tiergartenstrasse 15, D-69121, Heidelberg, Germany*
[5]*Dipartimento di Fisica 'Galileo Galilei', Università di Padova, Italy*
[6]*INFN, Sezione di Padova, Via Marzolo 8, I-35131 Padova, Italy*
[7]*Max-Planck-Institute for Astrophysics, Karl-Schwarzschild-Str. 1, D-85741 Garching, Germany*

Accepted 2009 March 5. Received 2009 March 4; in original form 2008 October 23

ABSTRACT

We have constructed the first all-sky cosmic microwave background (CMB) temperature and polarization lensed maps based on a high-resolution cosmological *N*-body simulation, the Millennium Simulation (MS). We have exploited the lensing potential map obtained using a previously developed map-making procedure which integrates along the line-of-sight the MS dark matter distribution by stacking and randomizing the simulation boxes up to $z = 127$, and which semi-analytically supplies the large-scale power in the angular lensing potential that is not correctly sampled by the *N*-body simulation. The lensed sky has been obtained by properly modifying the latest version of the LensPix code to account for the MS structures. We have also produced all-sky lensed maps of the so-called ψ_E and ψ_B potentials, which are directly related to the *electric* and *magnetic* types of polarization. The angular power spectra of the simulated lensed temperature and polarization maps agree well with semi-analytic estimates up to $l \leq 2500$, while on smaller scales we find a slight excess of power which we interpret as being due to non-linear clustering in the MS. We also observe how non-linear lensing power in the polarized CMB is transferred to large angular scales by suitably misaligned modes in the CMB and the lensing potential. This work is relevant in view of the future CMB probes, as a way to analyse the lensed sky and disentangle the contribution from primordial gravitational waves.

Key words: gravitational lensing – cosmic microwave background.

1 INTRODUCTION

The cosmic microwave background (CMB) is characterized both by *primary* anisotropies, imprinted at the last scattering surface at redshift $z \sim 1100$, and by *secondary* anisotropies caused along the way to us by density inhomogeneities and rescattering off electrons that are freed during the epoch of re-ionization, and heated to high temperature when massive structures virialize.

On one hand, the primary CMB anisotropies give direct insight into the structure of the very early Universe, and are one of the principal pillars on which the standard cosmological Λ cold dark matter (ΛCDM) model is founded. The temperature anisotropy power spectrum has now been measured to very high precision (e.g. Komatsu et al. 2009) yielding tight constraints on the basic parameters of the cosmological model.

On the other hand, one of the most important mechanisms that can generate secondary anisotropies is the weak gravitational lensing of the CMB, which arises from the distortions induced in the geodesics of CMB photons by gradients in the gravitational matter potential (Bartelmann & Schneider 2001; Lewis & Challinor 2006). The remapping of points produced by lensing induces non-Gaussianities in the observed CMB sky, and also changes the power spectra of the perturbations.

The CMB is also expected to be polarized at the ∼10 per cent level principally because of Thomson scattering of photons off free electrons during recombination. Thomson scattering generates linear polarization only, which is usually expressed in terms of the Stokes parameters *Q* and *U*. They can in turn be decomposed into coordinate independent E and B modes of polarization

⋆E-mail: carbone@ieec.uab.es (CC); bacci@sissa.it (CB); mbartelmann@ita.uni-heidelberg.de (MB); sabino.matarrese@pd.infn.it (SM); volker@MPA-Garching.MPG.DE (VS)

© 2009 The Authors. Journal compilation © 2009 RAS

Downloaded from http://mnras.oxfordjournals.org/ at INAF Brera Milano (Osservatorio Astronomico di Brera) on January 9, 2015

(e.g. Zaldarriaga & Seljak 1997) with opposite parities, the so-called 'electric' and 'magnetic' types of polarization. To linear order in perturbation theory, primordial scalar (density) perturbations can only generate E polarization, while primordial vector and tensor (gravitational waves) perturbations can generate both scalar E and pseudo-scalar B polarization (e.g. Seljak & Zaldarriaga 1997). In particular, *primary* B-mode polarization represents the imprints left from the primordial gravitational waves (GWs) on the CMB (Hu et al. 1998; Kamionkowski & Kosowsky 1999; Hu & Dodelson 2002): if initial fluctuations are created very early, e.g. during inflation so that the vector growth is damped, primary B modes are produced only by tensor perturbations that, being damped at last scattering by the horizon entering, produce the largest amount of temperature quadrupole anisotropy and, consequently, by Thomson scattering, the largest amount of polarization (Pritchard & Kamionkowski 2004). The primordial gravitational radiation is thought to have been generated by quantum fluctuations of the metric tensor during the inflationary era, with a strain amplitude proportional to the square of the inflation energy scale. Consequently, the indirect detection of this relic gravitational background via the direct observation of the primary B-mode polarization, as expected from future dedicated CMB missions by ESA and NASA,[1] will shed light on the physics of the very early Universe and will represent a powerful magnifier on the inflationary era and the very first moments in the existence of the Universe (Kamionkowski, Kosowsky & Stebbins 1997; Seljak & Zaldarriaga 1997; Zaldarriaga & Seljak 1997).

However, as for the CMB temperature, there are mechanisms also for the polarization that can produce *secondary* B modes, with the dominant one being again gravitational lensing, i.e. *cosmic shear* (CS), which distorts the primary CMB pattern, in particular converting E into B polarization (Zaldarriaga & Seljak 1998), even in case of absence of primary B modes. Although comparable, B modes from primordial GWs exhibit their peak at multipoles $l \approx 100$, corresponding to the degree scale, while, for lensed B modes, the peak is at $l \approx 1000$, corresponding to the arcmin scale. None the less, if the energy scale of inflation is $V^{1/4} \leq 4 \times 10^{15}$ GeV, the CS-induced curl represents a foreground for the $l \approx 50$–100 primordial GW-induced primary B polarization (Cabella & Kamionkowski 2005). This could limit the extraction of the gravity wave signal if not taken into account correctly (e.g. Seljak & Hirata 2004), even though forthcoming CMB probes will have in principle the sensitivity and the instrumental performance for the detection of the CMB anisotropies in total intensity and polarization.

A precise knowledge of the lensing effects would also provide new insights and constraints on the expansion history of the Universe, on the process of cosmological structure formation (Acquaviva & Baccigalupi 2006; Hu, Huterer & Smith 2006) and on the cosmological parameter estimation (Smith, Challinor & Rocha 2006a; Smith, Hu & Kaplinghat 2006b). In particular, for a correct interpretation of the data from the forthcoming Planck satellite,[2] it will be absolutely essential to understand and model the CMB lensing, as the satellite has the sensitivity for measuring the CMB lensing with good accuracy. We note that a first detection of CMB lensing in data from the *Wilkinson Microwave Anisotropy Probe* (*WMAP*[3]) combined with complementary data has already been claimed by Smith, Zahn & Dore (2007) and Hirata et al. (2008), and evidence for weak gravitational lensing of the CMB has been observed at $>3\sigma$ significance by Reichardt et al. (2009).

From the arguments above, it follows that the next generation CMB experiments will require a detailed lensing reconstruction and an accurate de-lensing methodology. One can try to reconstruct the gravitational lensing effects using the so-called quadratic and maximum-likelihood estimators (Hu & Okamoto 2002; Hirata & Seljak 2003), which allow to reproduce at some level of precision the lensing potential from the observed CMB itself, and to invert the photon geodesic remapping induced by the CS. Up to now these methodologies have been applied only to limited patches of sky (Amblard, Vale & White 2004) and/or under the hypothesis of a Gaussian distribution of the lensing sources (e.g. Seljak & Hirata 2004). However, this is only a first-order approximation, since the non-linear evolution of the cosmic structures induces non-Gaussian features in the lensing potential, features that in turn have an impact on the non-Gaussian statistic of the CMB produced by the point remapping caused by the CS itself on the CMB fluctuation pattern.

It is thus very interesting to test the performance of these estimators on full-sky, lensed CMB maps which do include the effects of the non-linear structure evolution at all the orders. This demands detailed simulated lensed CMB maps.

The increasing availability of high-resolution N-body simulations in large periodic volumes makes it possible to directly simulate the CMB distortions caused by weak lensing using realistic cosmological structure formation calculations. Our previous work (Carbone et al. 2008) represents a first step into this direction. Indeed, existing studies already give access to statistical properties of the expected all-sky CMB lensing signal (see e.g. Lewis 2005, and references therein), but these studies are based on 'semi-analytic' calculations that use approximate parametrizations of the non-linear evolution of the matter power spectrum. On the other hand, up to now N-body numerical simulations have been used to lens the CMB only in limited patches of sky (Das & Bode 2008), or to produce full-sky convergence maps confined to low redshifts $z \sim 1$ (Fosalba et al. 2008; Teyssier et al. 2008).

In Carbone et al. (2008), we have developed and described a procedure which gives access to the full statistics of the lensed CMB signal, including non-linear and non-Gaussian effects on the full sky. This should allow improvements in the methods for separating the different contributions to CMB anisotropies in the data, which would help substantially to uncover all the cosmological information in the forthcoming observations.

In this paper, we apply the methodology developed in Carbone et al. (2008) to the construction of all-sky, lensed simulated temperature and polarization maps. In Section 2, we describe the procedure utilized to lens, which is based on the simulated lensing potential and deflection-angle templates obtained in Carbone et al. (2008). In Section 3, we describe the resulting simulated lensed maps. In Sections 4 and 5, we apply statistical analyses to the obtained temperature and polarization lensed maps showing consistency and possible differences with respect to semi-analytical expectations. Finally, in Section 6 we draw the conclusions of this work and outline next steps and future applications.

2 CMB LENSING THROUGH THE MILLENNIUM SIMULATION

Weak lensing of the CMB deflects photons coming from an original direction $\hat{\boldsymbol{n}}'$ on the last scattering surface to a direction $\hat{\boldsymbol{n}}$ on the observed sky, so a lensed CMB field is given by $\tilde{X}(\hat{\boldsymbol{n}}) = X(\hat{\boldsymbol{n}}')$ in terms of the unlensed field $X = T, Q, U$ (e.g. Lewis 2005).

[1] See lambda.gsfc.nasa.gov for a complete list of operating and planned CMB experiments.
[2] www.rssd.esa.int/PLANCK
[3] See map.gsfc.nasa.gov

© 2009 The Authors. Journal compilation © 2009 RAS, MNRAS **396,** 668–679

Downloaded from http://mnras.oxfordjournals.org/ at INAF Brera Milano (Osservatorio Astronomico di Brera) on January 9, 2015

The displacement of the points is determined by the integral of the gravitational potential along the line-of-sight to the last scattering surface, as we review below.

In what follows, we will consider only the *small-angle scattering* limit, i.e. the case where the *change* in the comoving separation of CMB light rays, owing to the deflection caused by gravitational lensing from matter inhomogeneities, is small compared to the comoving separation between the *undeflected* rays. In this case, it is sufficient to calculate all the relevant integrated quantities, i.e. the so-called *lensing potential* and its angular gradient, the *deflection angle*, along the undeflected rays. This small-angle scattering limit corresponds to the Born approximation.

Adopting conformal time and comoving coordinates in a flat geometry (Ma & Bertschinger 1995), the integral for the projected lensing potential due to scalar perturbations with no anisotropic stress reads

$$\Psi(\hat{\boldsymbol{n}}) \equiv -2 \int_0^{r_*} \frac{r_* - r}{r_* r} \frac{\Phi(r\hat{\boldsymbol{n}}; \eta_0 - r)}{c^2} \, \mathrm{d}r \,, \tag{1}$$

where r is the comoving distance, $r_* \simeq 10^4$ Mpc is its value at the last-scattering surface, η_0 is the present conformal time and Φ is the physical peculiar gravitational potential generated by density perturbations (Hu 2000; Bartelmann & Schneider 2001; Refregier 2003; Lewis & Challinor 2006).

Actually, the lensing potential is formally divergent owing to the $1/r$ term near $r = 0$; none the less, this divergence affects the lensing potential monopole only, which can be set to zero, since it does not contribute to the deflection angle. In this way, the remaining multipoles take a finite value and the lensing potential field is well defined (Lewis & Challinor 2006). The vector $\hat{\boldsymbol{n}}'$ is obtained from $\hat{\boldsymbol{n}}$ by moving its end on the surface of a unit sphere by a distance $|\nabla_{\hat{n}}\Psi(\hat{\boldsymbol{n}})|$ along a geodesic in the direction of $\nabla_{\hat{n}}\Psi(\hat{\boldsymbol{n}})$, where $[1/r]\nabla_{\hat{n}}$ is the two-dimensional transverse derivative with respect to the line-of-sight pointing in the direction $\hat{\boldsymbol{n}} \equiv (\vartheta, \varphi)$ (Hu 2000; Challinor & Chon 2002; Lewis 2005). We assume $|\nabla_{\hat{n}}\Psi(\hat{\boldsymbol{n}})|$ to be constant between $\hat{\boldsymbol{n}}$ and $\hat{\boldsymbol{n}}'$, consistent with the Born approximation.

If the gravitational potential Φ is Gaussian, so is the lensing potential. However, the lensed CMB is non-Gaussian, as it is a second-order cosmological effect produced by cosmological perturbations on to CMB anisotropies, yielding a finite correlation between different scales and thus non-Gaussianity. This is expected to be most important on small scales, due to the non-linearity already present in the underlying properties of lenses.

In order to generate full-sky *T*, *Q*, *U* maps lensed by the matter distribution of the Millennium Simulation (MS), we have modified the publicly available LensPix code[4] (LP), which is described in Lewis (2005). In its original version, in fact, this code lenses the primary CMB intensity and polarization fields via a Gaussian realization, in the spherical harmonic domain, of the lensing potential power spectrum as extracted from the publicly available Code for Anisotropies in the Microwave Background (CAMB[5]). Our modification (hereafter referred to as 'MS-modified-LP') consists in forcing LP to deflect the CMB photons using the fully non-linear and non-Gaussian lensing potential realization obtained from the MS using the procedure briefly summarized here, which was presented by Carbone et al. (2008); we refer the reader to that paper for more detail.

The MS is a high-resolution *N*-body simulation for a ΛCDM cosmology consistent with the *WMAP* first year results (Spergel et al. 2003), carried out by the Virgo Consortium (Springel, Frenk & White 2005). It uses about 10 billion collisionless particles with mass $8.6 \times 10^8 \, h^{-1} \, \mathrm{M}_\odot$, in a cubic region $500 \, h^{-1}$ Mpc on a side which evolves from redshift $z_* = 127$ to the present, with periodic boundary conditions. Our map-making procedure is based on ray-tracing of the CMB photons in the Born approximation through the three-dimensional field of the MS peculiar gravitational potential. In order to produce mock lensing potential maps that cover the past light-cone over the full sky, we stack the peculiar gravitational potential grids around the observer (which is located at $z = 0$), exploiting the pre-computed and stored snapshots of the simulation. The spacing of the time outputs of the MS simulation is such that it corresponds to an average distance of $140 \, h^{-1}$ Mpc (comoving) on the past light-cone. We fully exploit this time resolution which, at high accuracy, allows us to avoid the adoption of time interpolation techniques, and use all the 63 outputs of the simulation along our integration paths. In practice, this means that the data corresponding to a particular output time are utilized in a spherical shell of average thickness $140 \, h^{-1}$ Mpc. Moreover, the total volume around the observer up to z_* is divided into spherical shells, each of thickness $500 \, h^{-1}$ Mpc. All the MS boxes falling into the same shell are translated and rotated with the same random vectors generating a homogeneous coordinate transformation throughout the shell, while the randomization vectors change from shell to shell. The peculiar gravitational potential at each point along a ray in direction $\hat{\boldsymbol{n}}$ is spatially interpolated from the pre-computed MS grid which possesses a spatial resolution of about $195 \, h^{-1}$ kpc. The deflection angle is computed along the line-of-sight as well, by numerically evaluating the gravitational potential gradient and interpolating at each point along the line-of-sight (Carbone et al. 2008).

Being repeated on scales larger than the box size, the resulting weak lensing distortion lacks large-scale power, which manifests itself in the lensing potential power spectrum as an evident loss of large-scale power with respect to semi-analytic expectations, which is most noticeable for multipoles smaller than $l \simeq 400$. This has been cured by augmenting large-scale power (LS-adding) directly in the angular domain, a procedure which we exploit here as well. More specifically, we have implemented the LS-adding technique directly into the LensPix code as we now explain. We have again split the spherical harmonics domain into two multipole ranges: $0 \leq l \leq 400$, where the MS fails in reproducing the correct lensing potential power due to the limited box size of the simulation, and $l > 400$, where instead the power spectrum is reproduced correctly by the MS (see Fig. 1). On the latter interval of multipoles, we have extracted the corresponding ensemble Ψ_{lm}^{MS} of lensing-potential spherical harmonic coefficients produced by the MS lens distribution. We have modified the LensPix code so that it reads and uses these MS harmonic coefficients on the corresponding range of multipoles. On the interval $0 \leq l \leq 400$, instead, we let LensPix generate its own ensemble of spherical harmonic coefficients Ψ_{lm}^{LP}, which are a realization of a Gaussian random field characterized by the CAMB semi-analytic lensing-potential power spectrum (including the estimate of the contribution from non-linearity; Smith et al. 2003) inserted as input in the parameter file of LP.

Since on low multipoles the effects of the non-Gaussianity from the non-linear scales are negligible and the Ψ_{lm} are independent, every time that we run the MS-modified-LP, we generate a joined ensemble of $\tilde{\Psi}_{lm}$, where $\tilde{\Psi}_{lm} = \Psi_{lm}^{\mathrm{LP}}$ for $0 \leq l \leq 400$ and $\tilde{\Psi}_{lm} = \Psi_{lm}^{\mathrm{MS}}$ for $l > 400$.

This technique achieves two goals: first, it reproduces correctly the non-linear and non-Gaussian effects of the MS non-linear dark

[4] http://cosmologist.info/lenspix/
[5] http://camb.info/

Downloaded from http://mnras.oxfordjournals.org/ at INAF Brera Milano (Osservatorio Astronomico di Brera) on January 9, 2015

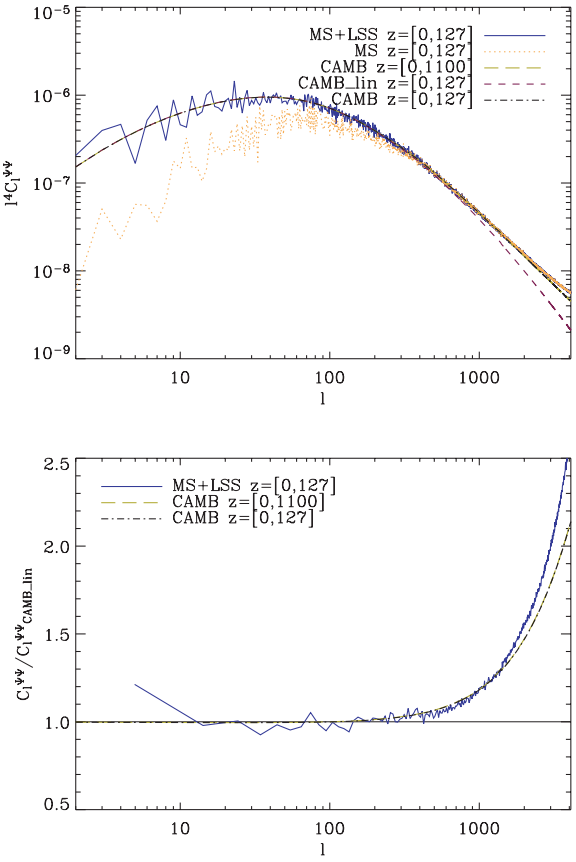

Figure 1. Top panel: the dotted orange line represents the simulated lensing potential power spectrum obtained via line-of-sight integration across the MS dark matter distribution up to $z = 127$. The blue solid line is the same as the orange dotted one after reinstating the large-scale power with the use of the LS-adding technique. The dot–dashed black line represents the power spectrum of the lensing potential obtained with the CAMB code stopping the line-of sight integration at $z = 127$, and including an estimate of the non-linear contributions (Smith et al. 2003). The long-dashed light-green line is the same as the dot–dashed black one with line-of-sight integration up to $z = 1100$. Finally, the dashed violet line represents the linear lensing potential power spectrum from the CAMB code in the linear approximation and integrating up to $z = 127$. Bottom panel: the ratios between the power spectra shown in the top panel and the CAMB linear lensing potential spectrum up to $z = 127$. It is worth to note that there is no difference using $z = 1100$ or 127 for the semi-analytical expectations.

matter distribution on multipoles $l > 400$, including at the same time the contribution from the large scales at $l \leq 400$, where the lensing potential follows mostly the linear trend as shown from the light-green dot–dashed line in Fig. 1. Secondly, it allows to take correctly into account the cross-correlation between the temperature and the lensing-potential (e.g. Lewis & Challinor 2006) due to the Integrated Sachs-Wolfe (ISW) effect on the low multipoles, i.e. on the large scales (this effect is instead negligible at $l \gtrsim 200$; Afshordi 2004). In fact, as it happens for the semi-analytic contribution to the lensing-potential, also the primary temperature and polarization fields are generated by LP as Gaussian realizations, in the harmonic domain, of the corresponding power spectra obtained by CAMB, which correctly includes the contribution to the temperature from the ISW effect. We emphasize that we always run CAMB using the same cosmological parameters as the MS specified in Section 2, and, for consistency with the MS map-making procedure, we have fixed the maximum redshift of the line-of-sight integration for the CAMB lensing sources at $z_{\rm max} = 127$. Indeed, the lensing power from even higher redshifts is negligible for CMB lensing, as we show in Fig. 1 where the light-green long-dashed line overlaps the black dash–dotted line perfectly.

On multipoles $l > 400$, the cross-correlation between the lensing-potential and the temperature is negligible, even if there could be some residual contribution coming from the non-linear Rees–Sciama effect. In this work, we do not consider the cross-correlation due to this second-order effect.

To generate the lensed *T*, *Q*, *U* fields from the MS-modified-LP code, we adopt the interpolation scheme described in appendix E 4 of Hamimeche & Lewis (2008), using a high value of the multipole $l_{\rm max}$ to maximize the accuracy. This allows running the simulation several times without excessive consumption of CPU time and memory. We work under the null hypothesis that tensor modes are absent in the early Universe, so that the produced B-mode polarization is due only to the power transfer from the primary scalar E modes into the lens-induced B modes. We choose $l_{\rm max} = 6143$ and interp-factor $= 1.5$, effectively the same resolution as HEALPix[6] with pixelization parameter $N_{\rm side} = 2048$, which corresponds to an angular resolution of $\sim$1.72 arcmin (Gorski et al. 2005), with $12N_{\rm side}^2$ pixels in total.

For comparison and testing, we also generate the corresponding unmodified-LP and unlensed *T*, *Q*, *U* maps, by choosing the same positive seed in the LP parameter file (hereafter 'unmodified-LP' stands for the results obtained by lensing the sky with the original unmodified version of the LensPix code).

3 SIMULATED LENSED MAPS

The subtraction of the unlensed CMB maps from the corresponding lensed CMB maps allows highlighting the dark matter distribution which causes the gravitational deflection of the CMB photons. In the upper and middle panels of Fig. 2, we show the resulting difference temperature and polarization maps for a particular seed choice and for the MS-modified-LP case only, since the arcmin-scale differences with respect to the unmodified-LP case are not visible by the naked eye. It is worth noting how the distribution of the deflection-angle modulus (lower panel) reflects itself in the distribution of the temperature difference map (upper panel) and in the distribution of the map of the polarization modulus $\Delta P = \sqrt{\Delta Q^2 + \Delta U^2}$ (middle panel), which has been obtained from the difference *Q* and *U* maps. Unfortunately, since the primary unlensed CMB is unknown, the difference maps cannot be directly observed. Anyway, the simulated difference maps can help to physically and visually understand how large-scale correlations are imprinted on the CMB due to the large-scale modes in the deflection field, and to catch effects that are not observable due to primary unlensed CMB.

The temperature and polarization difference maps have the peculiarity of including all the information inferred from weak lensing on the primary unlensed CMB. None the less, it is well known that the lensed B modes of polarization are more sensitive to the non-linear evolution of the cosmic structures than the T, Q and U modes separately (Lewis 2005). The difference between the unmodified-LP and MS-modified-LP cases lies exactly at the non-linear level, since the lensing-potential realizations differ at multipoles $l > 400$ in the spherical harmonic space for the two cases. Moreover, from Fig. 1, we observe that the MS lensing potential shows an excess of power on $l > 2500$ with respect to the CAMB approximation, and,

[6] http://healpix.jpl.nasa.gov/

© 2009 The Authors. Journal compilation © 2009 RAS, MNRAS **396,** 668–679

Downloaded from http://mnras.oxfordjournals.org/ at INAF Brera Milano (Osservatorio Astronomico di Brera) on January 9, 2015

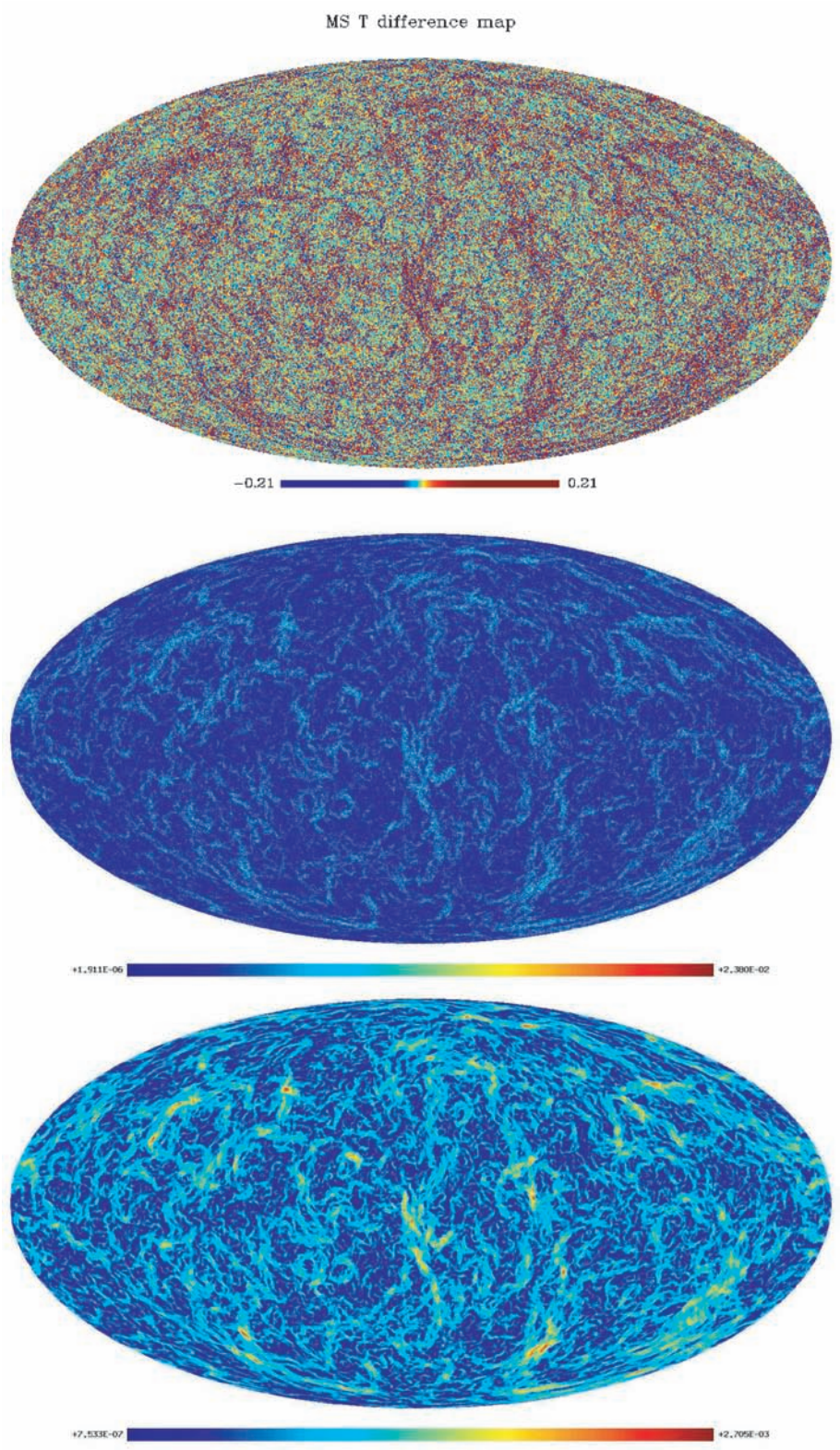

Figure 2. Top panel: difference T map between the lensed and unlensed T fields obtained by supplying the LensPix code with the spherical harmonic coefficients extracted from the MS lensing potential map and by implementing in it the LS-adding technique, as described in the text. Units in *mK*. A histogram equalized colour mapping has been used to increase the contrast. Middle panel: modulus of the polarization $\Delta P \equiv \sqrt{\Delta Q^2 + \Delta U^2}$, where ΔQ and ΔU are the difference Q and U maps obtained using the same technique as for the T difference map of the top panel. Units in *mK*. Bottom panel: map of the deflection-angle modulus obtained as angular gradient of the lensing-potential whose power spectrum is represented by the solid blue line in Fig. 1.

Downloaded from http://mnras.oxfordjournals.org/ at INAF Brera Milano (Osservatorio Astronomico di Brera) on January 9, 2015

as already pointed out, the non-linear dark matter evolution may enhance the level of non-Gaussianity present in the lensed CMB maps.

Consequently, in order to verify if the different distributions of the lensing potential in the MS-modified-LP and unmodified-LP cases could visibly affect the lensed polarization distributions, we have constructed the full-sky maps of the scalar ψ_E and pseudo-scalar ψ_B potentials, which are related to the Q and U Stokes parameters as follows (Bunn et al. 2003):

$$Q + iU = \eth\eth(\psi_E + i\psi_B), \tag{2}$$

$$Q - iU = \bar{\eth}\bar{\eth}(\psi_E - i\psi_B), \tag{3}$$

where the spin-raising $\eth$ and spin-lowering $\bar{\eth}$ operators on the sphere are defined as (Newman & Penrose 1966)

$$\eth = -\sin^s\theta\left[\frac{\partial}{\partial\theta} + i\csc\theta\frac{\partial}{\partial\phi}\right]\sin^{-s}\theta, \tag{4}$$

$$\bar{\eth} = -\sin^{-s}\theta\left[\frac{\partial}{\partial\theta} - i\csc\theta\frac{\partial}{\partial\phi}\right]\sin^{s}\theta, \tag{5}$$

and s is the spin of the function to which the operator is applied. The quantities ψ_E and ψ_B are directly related to the electric and magnetic types of polarization, since their spherical harmonic coefficients can be written in terms of the harmonic coefficients of the E and B modes, respectively

$$\psi_E = -\sum_{lm}[(l-2)!/(l+2)!]^{1/2}a_{E,lm}Y_{lm}, \tag{6}$$

$$\psi_B = -\sum_{lm}[(l-2)!/(l+2)!]^{1/2}a_{B,lm}Y_{lm}. \tag{7}$$

The ψ_E and ψ_B potentials are very useful for real space calculations and, exploiting the HEALPix routine SYNFAST (Gorski et al. 2005), we have produced the corresponding maps as synthetic realizations, using the E, B spherical harmonic coefficients extracted (via the HEALPix routine ANAFAST) from the lensed Q, U simulated maps and multiplied by the prefactors of equations (6) and (7), respectively. On high multipoles, these prefactors have the asymptotic form $[(l-2)!/(l+2)!]^{1/2} \sim l^{-2}$, consequently their effect is to suppress the small-scale power with respect to the E- and B-mode cases, and to make the large-scale structure differences much more evident.

In fact, looking at Figs 3 and 4, we observe that the lensed ψ_E and ψ_B difference maps have a *degree*-scale distribution which differs in the MS-modified-LP and unmodified-LP cases, even if the corresponding lensing-potential maps differ on *arcmin* scales ($l > 400$). This result is more expected in the B-mode case

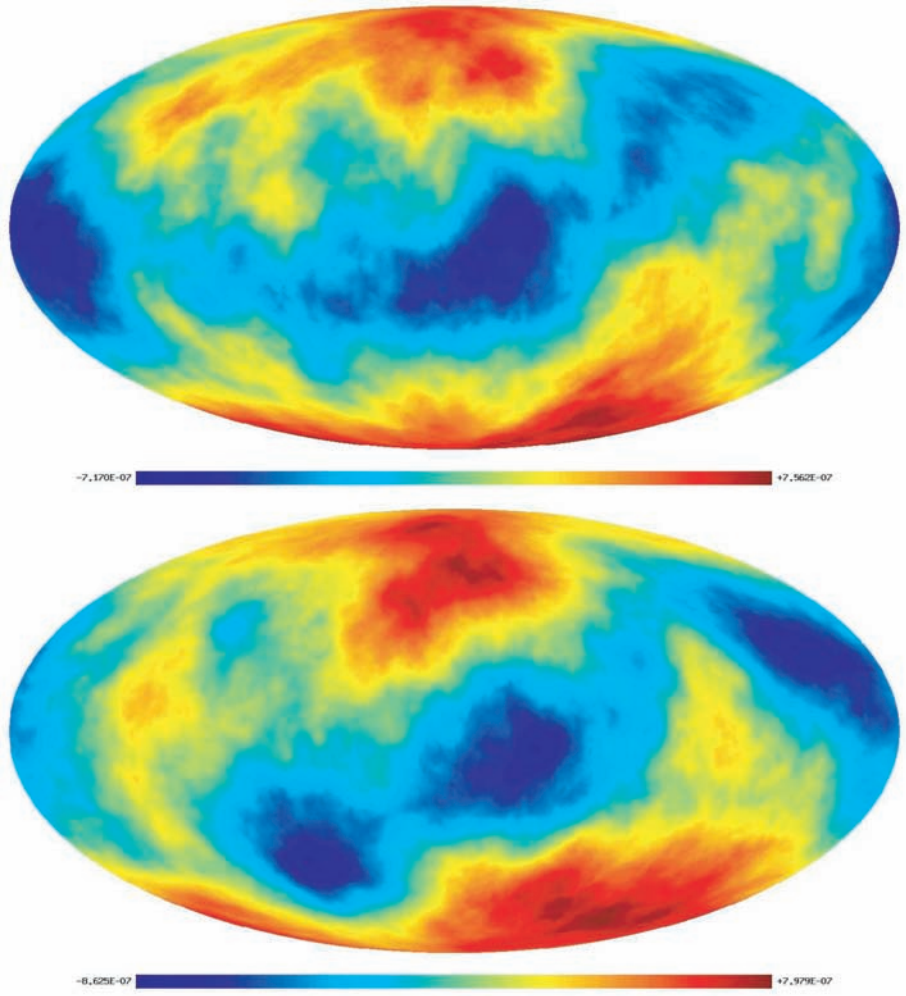

Figure 3. Difference maps between the ψ_E lensed and unlensed fields, obtained in the MS-modified-LP case (upper panel) and in the unmodified-LP case (lower panel). Units in *mK*.

Downloaded from http://mnras.oxfordjournals.org/ at INAF Brera Milano (Osservatorio Astronomico di Brera) on January 9, 2015

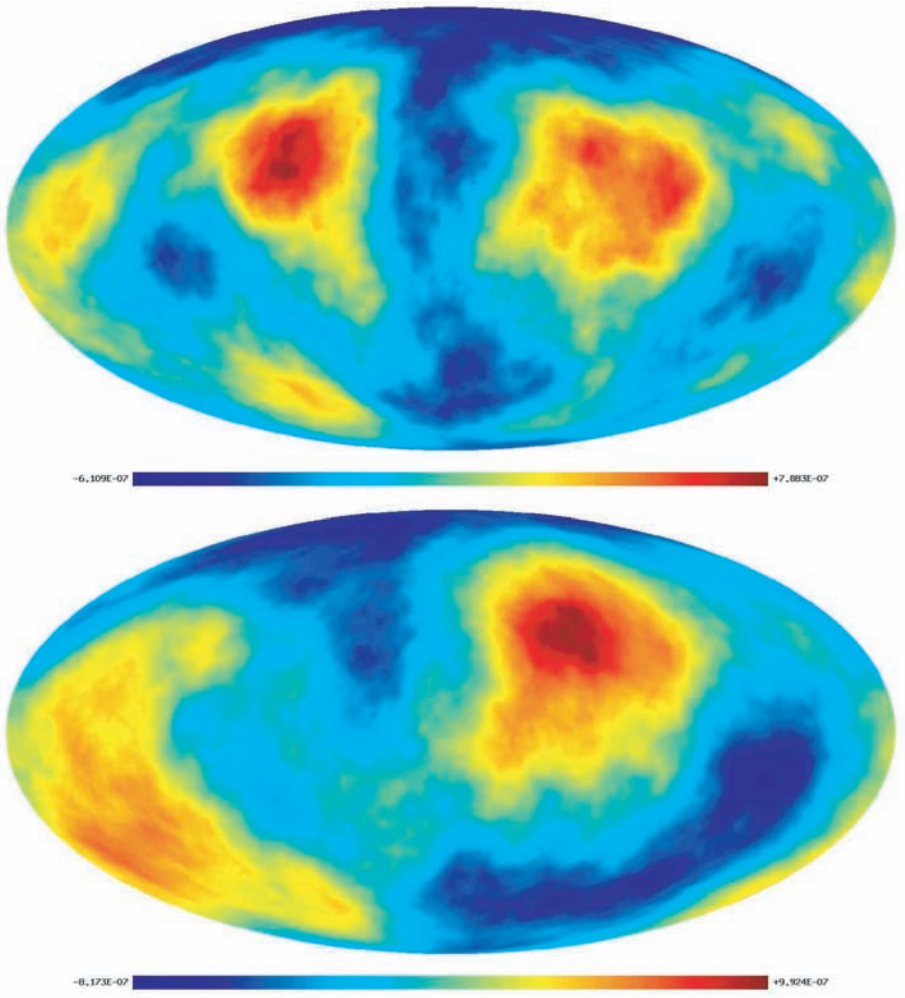

Figure 4. Difference maps between the ψ_B lensed and unlensed fields, obtained in the MS-modified-LP case (upper panel) and in the unmodified-LP case (lower panel). Units in *mK*.

since it is well known that the non-linear density field introduces $\sim$10 per cent corrections to the lens-induced B-mode power on all scales (Lewis & Challinor 2006), so that multipoles $l > 400$ will affect the ψ_B-field realizations on larger scales too. The same is instead less obvious in the E-mode case.

In order to understand the reason of the different large-scale distribution of these maps, we have also produced the lensed temperature, ψ_E and ψ_B fields using a Gaussian lensing-potential distribution which includes only the scales that correspond to multipoles up to $l_{lp} = 400$ in the spherical harmonic domain (where the subscript 'lp' stands for lensing potential). For comparison among the figures, we have used the same seed as for the fully ($0 \leq l_{lp} \leq 6143$) lensed maps, even if the results have been tested for different seeds. In Fig. 5, we show the ratios between the signals corresponding to the two cases, both for the lensed and difference maps.

In particular, if we consider the lensed T- and E-mode power spectra (top panel of Fig. 5) which include the contribution from the primary CMB, we do not observe any substantial difference on the large scales between the two cases $0 \leq l_{lp} \leq 400$ and $0 \leq l_{lp} \leq 6143$, so that on large scales the lensed electric polarization appears not to be much affected by the non-linear scales in the same way as the lensed temperature is. The *B* case is different since we are working with the null hypothesis of vanishing primary magnetic polarization, so that we are considering here only lens-induced B modes.

None the less, if we consider the power spectra extracted from the difference *T* and ψ_E maps (where we are subtracting the primary CMB), and again take the ratios between the signals in the two cases $0 \leq l_{lp} \leq 400$ and $0 \leq l_{lp} \leq 6143$ (lower panel of Fig. 5), we see that on large scales the E-mode polarization, cleaned of the primary signal, gets power from the smaller scales. In particular we see that, in the E and B cases, multipoles larger than $l_{lp} = 400$ transfer about 100 per cent of the power to the low multipoles $l \lesssim 100$, i.e. on scales large enough for the flat-sky approximation to be inadequate. This transfer of power towards low multipoles is possible only for peculiar alignment angles between the unlensed E mode and the lensing structures, i.e. for almost, but not quite aligned modes. This is analogous to the long-wavelength beat mode one obtains from superposing two oscillations with two almost equal frequencies. We do not observe the same effect when we consider the ratio between the signals extracted from the temperature difference maps in the two cases $0 \leq l_{lp} \leq 400$ and $0 \leq l_{lp} \leq 6143$, where the transfer of power is less than 10 per cent on $l \lesssim 100$. As we move to larger multipoles instead, the power transfer decreases and, for $400 \leq l \leq 2000$, the lensed *E* trend starts converging to the lensed temperature one, while the power of the lens-induced B modes goes

Downloaded from http://mnras.oxfordjournals.org/ at INAF Brera Milano (Osservatorio Astronomico di Brera) on January 9, 2015

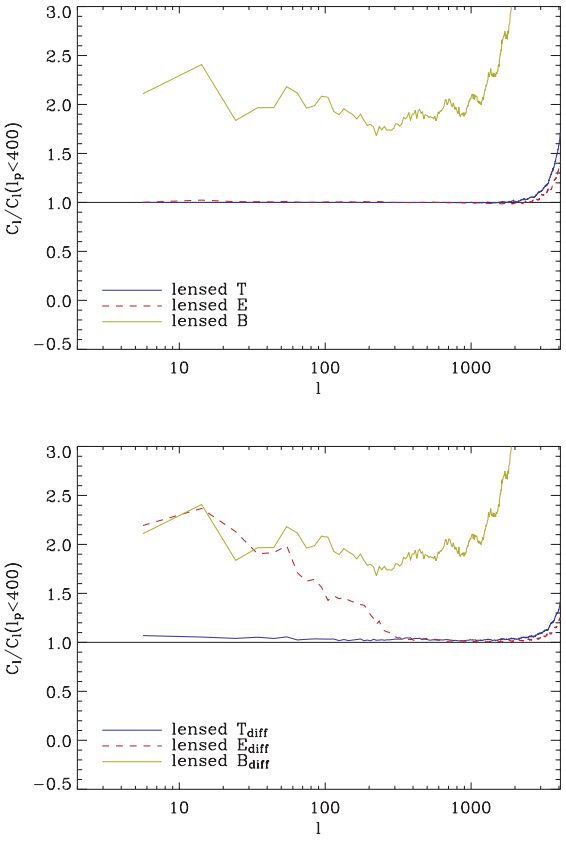

Figure 5. Top panel: the dot–dashed light-green line represents the ratio between the lens-induced B power spectrum, which is obtained using the multipole range $0 \leq l_{lp} \leq 6143$ for the spherical harmonic coefficients of the lensing potential, and the spectrum obtained using only $0 \leq l_{lp} \leq 400$. The solid blue line and the dashed red line represent these ratios in the T and E cases, respectively. Bottom panel: the same as the upper panel when we calculate these ratios for the temperature and polarization power spectra extracted from the difference T, Q and U maps, in the $0 \leq l_{lp} \leq 6143$ and $0 \leq l_{lp} \leq 400$ cases, respectively.

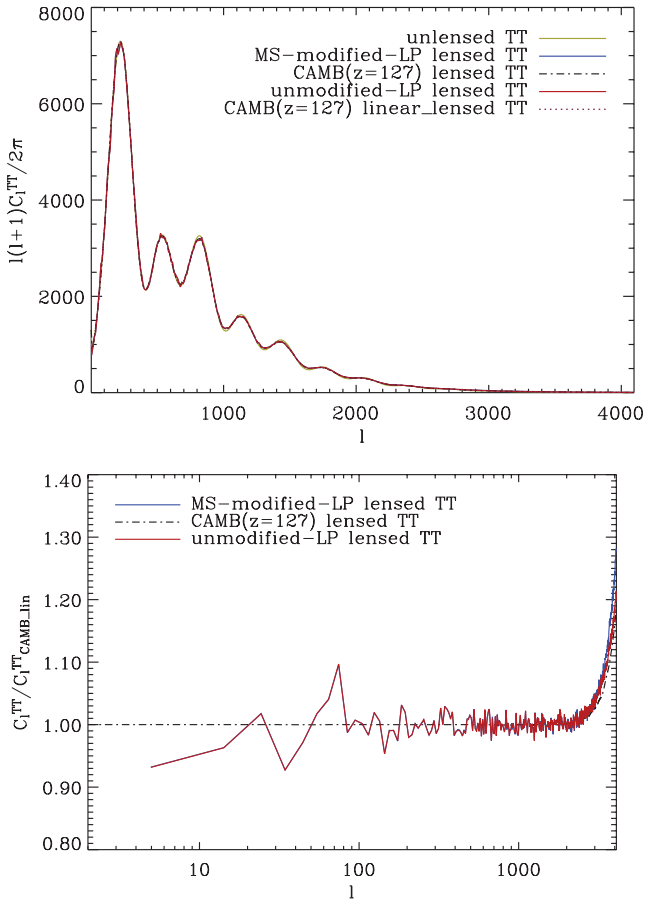

Figure 6. Top panel: temperature power spectra (μK^2) for the different cases described in the text. Bottom panel: temperature power spectrum ratios with respect to the linear lensed case.

on increasing with the multipoles, still fed by the non-linear scales in the lensing-potential at $l_{lp} > 400$.

Therefore, we conclude that in Figs 3 and 4 the different degree-scale distributions which characterize the MS-modified-LP and unmodified-LP $\psi_E(\psi_B)$ difference map realizations (even though the corresponding lensing-potential realizations differ only on $l_{lp} > 400$) represent the imprints of the power transfer from smaller to larger scales induced by the lensing remapping on to the lensed E and B signals cleaned of the primary CMB, in a way which differs from what happens to the lensed temperature.

4 ANGULAR POWER SPECTRA

In this Section, we perform several quantitative analyses of the obtained results. Our principal aim is to test the consistency and quantify the differences between the theoretical expectations and the findings from our simulation procedure.

As a first check, we have extracted from the corresponding maps the angular power spectra of the MS-modified-LP and unmodified-LP simulated lensed T, E and B components, together with the TE lensed cross-correlation power spectrum. This is simply done with the use of ANAFAST, adopting the correct deconvolution rules for the HEALPIX pixel window functions, and with equations (6) and (7) relating the spherical harmonic coefficients of the ψ_E and ψ_B potentials to the corresponding coefficients of the E and B modes.

We have also checked that the MS-modified-LP and unmodified-LP simulated spectra extracted directly from the maps agree with the ones obtained as direct outputs of the MS-modified-LP and unmodified-LP codes, respectively. Moreover, to test the accuracy, we have compared all the angular power spectra with the lensed CMB power spectra obtained using the all-sky correlation function technique implemented in CAMB (Challinor & Lewis 2005). These angular power spectra are shown in the upper panels of Figs 6–9, respectively, together with the CAMB unlensed and the linearly lensed spectra, where the latter are obtained in the linear approximation of the cosmic structure growth. Moreover, in the lower panels of the same figures we show the ratios between the simulated lensed CMB angular spectra with respect to the corresponding linear signal.

In the TT, EE and TE cases, it is clearly visible that CMB lensing smears out the acoustic peaks by transferring power from larger to smaller scales. Moreover, since we are working under the null hypothesis of vanishing intrinsic tensor modes, Fig. 8 represents the power spectrum of the lens-induced B modes into which part of the primary E modes has been converted as a result of the displacements and distortions induced from the gravitational deflection on to the electric-type polarization field.

As Figs 6, 7 and 9 show, for all the lensed TT, EE and TE angular spectra, and for all multipole orders up to $l \leq 3500$, we

Downloaded from http://mnras.oxfordjournals.org/ at INAF Brera Milano (Osservatorio Astronomico di Brera) on January 9, 2015

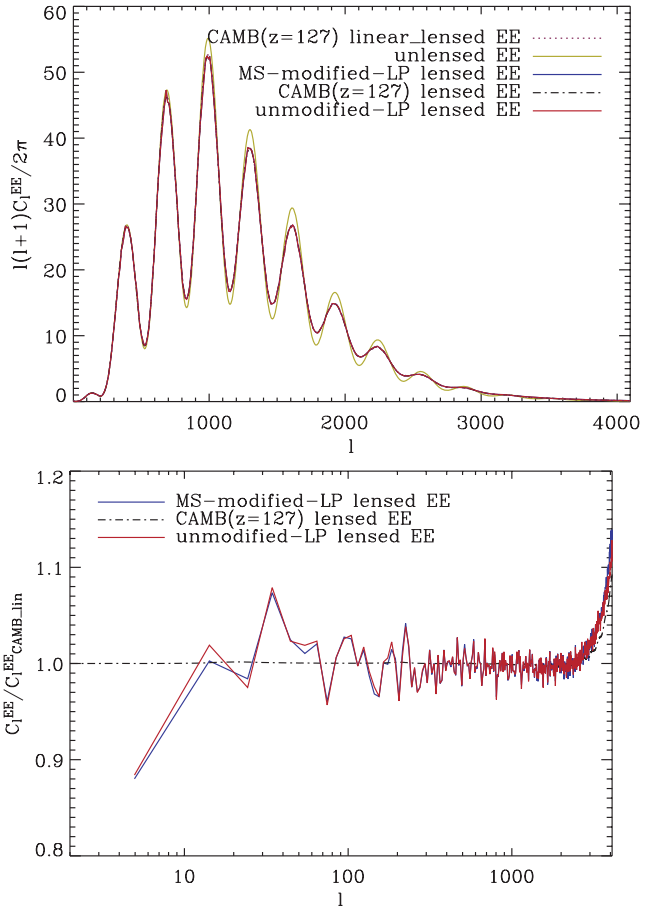

Figure 7. Top panel: E-mode power spectra (μK^2) for the different cases described in the text. Bottom panel: E-mode power spectrum ratios with respect to the linear lensed case.

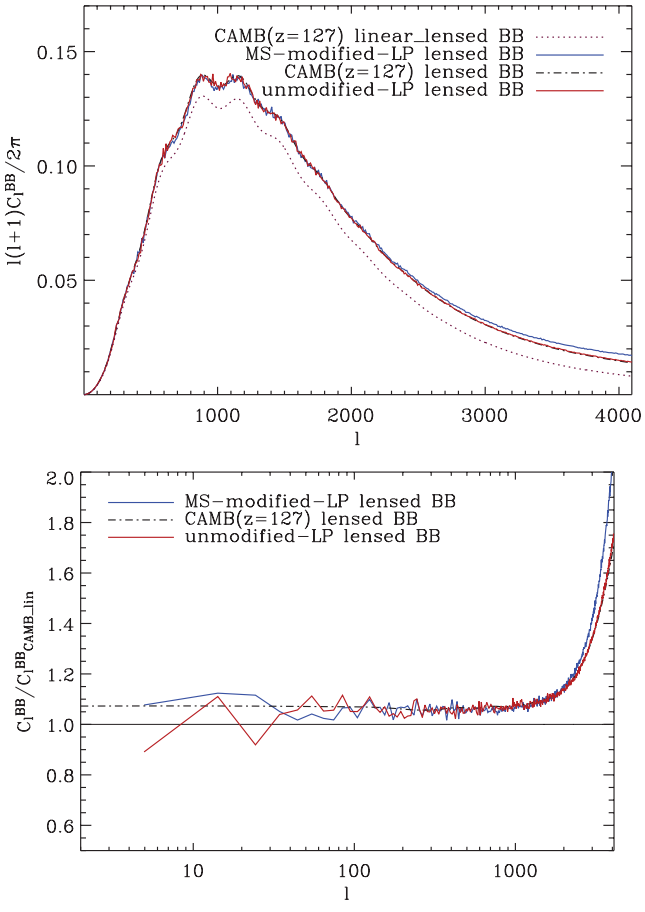

Figure 8. Top panel: lens-induced B-mode power spectra (μK^2) for the different cases described in the text. Bottom panel: lens-induced B-mode power spectrum ratios with respect to the linear lensed case.

observe a mostly perfect agreement between the MS-modified-LP simulated signals and the unmodified-LP and CAMB ones, where the non-linear structure evolution is semi-analytically taken into account. On the very large multipoles $l > 3000$, a small difference appears between the CAMB and unmodified-LP lensed *TT, EE* and *TE* spectra, probably due to a numerical effect deriving from the different computational machinery implemented in CAMB and LensPix, respectively. The non-linear effects start to be important at $l > 2500$, according to the semi-analytical expectations, and, on multipoles $l \sim 4000$, which correspond to angular scales of few arcmin, they grow up to ∼20 per cent for the lensed temperature and up to ∼10 per cent for the lensed electric polarization. Moreover, the excess of power present in the MS lensing-potential power spectrum at multipoles $l \geq 2500$ (see Fig. 1) manifests itself as a slight excess of power in the MS-modified-LP lensed *TT* and *EE* spectra at $l \geq 3500$. In particular, at $l = 4096$, the non-linearities present in the MS produce a ∼6 per cent excess in the lensed temperature and a ∼1.3 per cent excess in the lensed electric polarization, with respect to the unmodified-LP case.

On the other hand, the excess of power due to the MS non-linearities is much more evident in the angular power spectrum of the magnetic component (see Fig. 8) where this effect starts already at $l \sim 2500$ and grows up to ∼14 per cent at $l = 4096$, with respect to the unmodified-LP case. Moreover, the non-linear effects, which in the lensing potential appear at $l \geq 400$, spread on all the scales of the lens-induced B-mode spectrum, being already of the order of ∼7.5 per cent on all the multipoles $l \leq 1000$, and growing up to more than ∼70 per cent at $l = 4096$. As we have previously noted, this non-linear effect on the magnetic polarization is simply explained considering that the lens-induced B modes are very sensitive to the non-linear evolution of the cosmic structures.

For what concerns the non-linear effects, as noted already in Section 3, it is important to stress again that, when considering the power spectra extracted from the difference maps (in which the primary CMB has been subtracted), we note a very similar large-scale behaviour between the electric and magnetic polarization, which strongly differs from the temperature trend. In order to analyse this effect, we have produced the *linearly*-lensed *T, Q, U* maps and subtracted the unlensed field. In Fig. 10, we show the two cases: the ratios of the lensed *T*, *E*, *B* spectra with respect to the corresponding spectra extracted from the linearly lensed maps, and the same ratios extracted from the corresponding lensed and linearly lensed *difference* maps. While in the first case (top panel), the transfer of power from small scales to large scales is only visible in the lens-induced B-mode spectrum, in the second case (bottom panel) this power transfer is also observable in the lensed E-mode spectrum, with the same amount of ∼7.5 per cent up to $l \lesssim 100$ as for the lens-induced B modes. The same does not occur to the lensed temperature even after subtracting the unlensed CMB. Finally, moving to higher multipoles, the *E* and *T* signals converge to the same trend, while the *B* signal keeps on growing because of the non-linear power.

Downloaded from http://mnras.oxfordjournals.org/ at INAF Brera Milano (Osservatorio Astronomico di Brera) on January 9, 2015

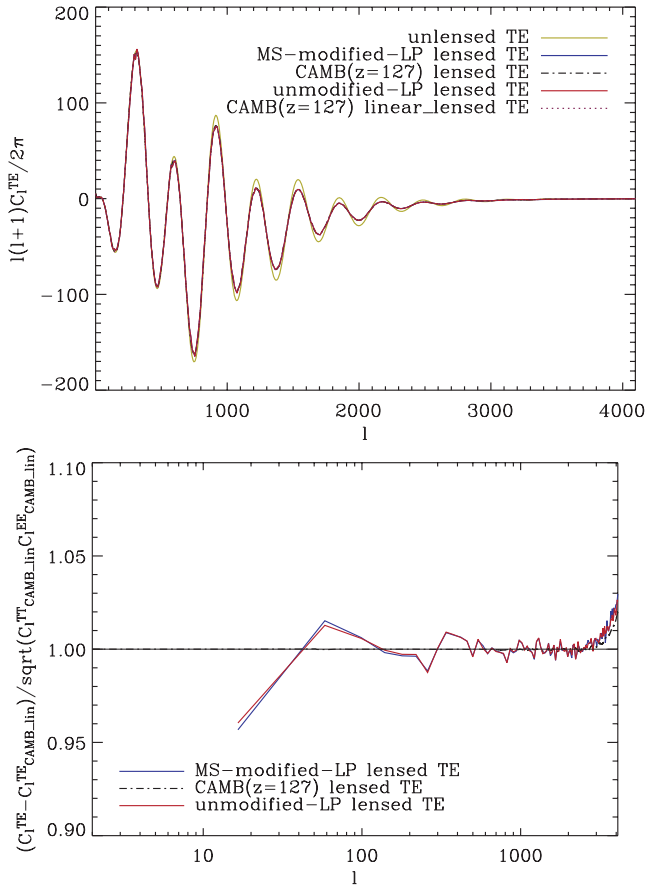

Figure 9. Top panel: *T*-*E* cross-power spectra (μK^2) for the different cases described in the text. Bottom panel: the fractional change in the lensed *T*-*E* cross-power spectrum due to the non-linear matter evolution for the different cases described in the text.

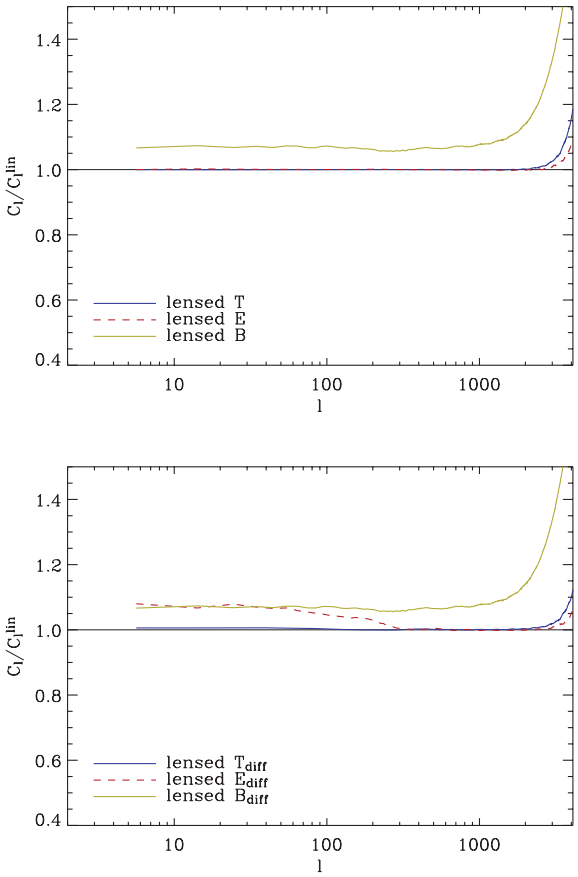

Figure 10. Top panel: the dot–dashed light-green line represents the ratio between the lens-induced *B* power spectrum, which is obtained including the non-linear cosmic structure evolution, and the spectrum obtained in the linear limit. The solid blue line and the dashed red line represent these ratios in the *T* and *E* cases, respectively. Bottom panel: the same as the upper panel when we calculate these ratios for the temperature and polarization power spectra extracted from the difference T, Q and U maps, in the linear and non-linear cases, respectively.

5 ONE-POINT STATISTICS

As a second analysis, we compare the one-point probability density distributions (PDFs) of the lensed *T*, *Q*, *U* maps with the PDFs of Gaussian distributions randomly generated using the corresponding mean and standard deviation values of the lensed maps. The PDFs of both the simulated MS-modified-LP and unmodified-LP *T*, *Q*, *U* maps do not show evidence of non-Gaussian features (upper panel of Fig. 11), and are consistent with the unlensed temperature and polarization distributions within a few per cent. This occurs thanks to the high angular resolution of our maps (see e.g. Kesden, Cooray & Kamionkowski 2002), and is understandable because the main effect of CMB lensing is to transfer power among different scales, without generating new power (and we assume that the primary unlensed CMB field has a Gaussian distribution).

On the other hand, it is well known that the remapping induced by lensing on to the *T*, *Q*, *U* fields generates a non-Gaussian signature in the lensed sky which is optimally characterized by higher order statistics as the bispectrum and trispectrum (see e.g. Lewis & Challinor 2006, and references therein). This is mainly due to the fact that the lensed CMB can be considered as a function of two fields, the unlensed sky and the lensing potential, which in first approximation can be assumed to be Gaussian (unmodified-LP case), even if the non-linear evolution of large-scale structures produces non-Gaussian features in the distribution of the projected potential (MS-modified-LP case). In particular, the non-Gaussianity associated with the large-scale structure induces non-Gaussian contributions to the distribution of the lensing potential such that its *n*-point correlator in Fourier space will be non-vanishing for some value of *n*, and this, in turn, has an impact on the connected part of the *n*-point correlators of the lensed CMB (see e.g. Kesden et al. 2002). Anyway, there exist also other phenomena that can produce non-Gaussian effects in the lensed CMB, for instance the correlations between CMB lensing and the Sunyaev–Zeldovich effect.

Here, as a first characterization of the non-Gaussianity strength produced by CMB lensing, we consider the PDFs of the *difference T*, *Q*, *U* maps. In this way, we subtract the unlensed Gaussian sky and isolate the non-Gaussian term which physically generates the non-Gaussian signatures in the lensed CMB. The obtained PDF in the temperature case is showed in the lower panel of Fig. 11 (the *Q* and *U* cases have a similar trend).

The PDFs of the difference maps are characterized by a kurtosis excess with respect to Gaussian distributions randomly generated with the same mean and standard deviation values. More precisely, averaging over different realizations, the kurtosis excess is ∼2.41 for the difference *T* map, ∼2.14 for the difference *Q* map and ∼2.16 for the difference *U* map. Actually, we would expect that the excess

Downloaded from http://mnras.oxfordjournals.org/ at INAF Brera Milano (Osservatorio Astronomico di Brera) on January 9, 2015

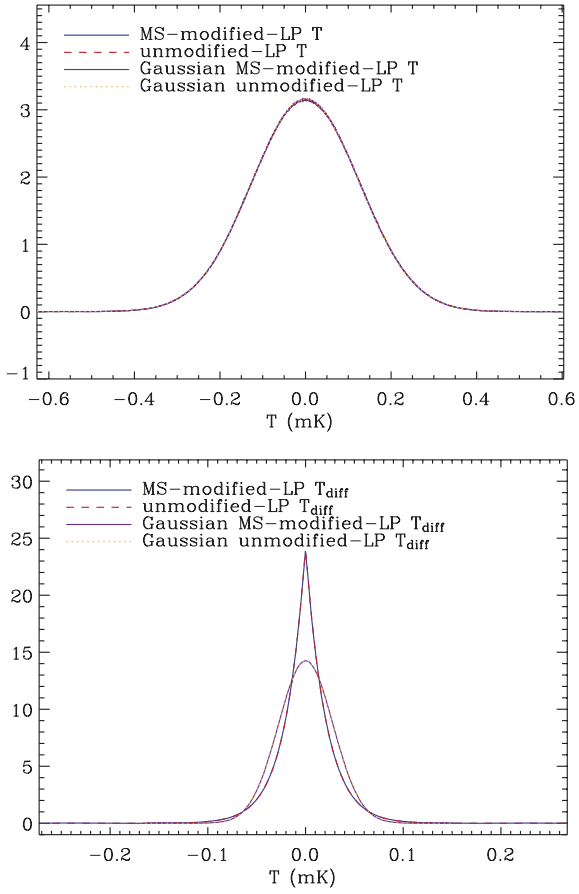

Figure 11. Top panel: the PDF of the temperature maps obtained in the MS-modified-LP and unmodified-LP cases compared to the PDF of Gaussian distributions with the corresponding mean value and standard deviation, respectively. Bottom panel: the same as in the upper panel for the PDFs of temperature difference maps.

of non-linearities in the dark matter distribution of the MS should show up as an excess of non-Gaussianity in the MS-modified-LP lensed difference *T*, *Q*, *U* maps, with respect to the unmodified-LP case. However, the one-point statistic is probably unable to capture this effect, and Fig. 11 shows in fact that there is not a significant difference between the unmodified-LP and MS-modified-LP cases. In this respect, we believe that a more suitable estimator should be developed in order to detect the contribution from the non-linear structure evolution to the total non-Gaussian statistics of the lensed maps. We reserve this analysis for future work.

6 CONCLUSIONS

We have constructed the first all-sky CMB temperature and polarization lensed maps based on a high-resolution cosmological *N*-body simulation, the MS.

To this purpose, we have exploited the lensing potential map obtained using the map-making procedure developed in Carbone et al. (2008) which integrates along the line-of-sight the MS dark matter structures by stacking and randomizing the simulation boxes up to $z = 127$. Specifically, we have modified the LensPix code (Lewis 2005) by supplying it with the spherical harmonic coefficients extracted from the MS lensing potential map and by implementing directly in the code itself the large-scale structure adding technique (see Carbone et al. 2008) which allows to reinstate the large-scale power in the angular lensing potential that is not correctly sampled by the *N*-body simulation. In this way, we also preserve the correct correlation between the lensing potential and the ISW effect on multipoles $l \leq 400$ in the simulated temperature anisotropies.

Using our modified version of the LensPix code, we have constructed lensed CMB simulated maps with ∼5 million pixels and an angular resolution of ∼1.72 arcmin, based on potential fields calculated on 2560^3 mesh cells from the MS.

After subtraction of the unlensed maps, the corresponding lensed *T*, *Q*, *U* simulated maps reflect clearly the same large-scale structure which is present in the modulus of the angular gradient of the lensing potential map (see Fig. 2).

We have also constructed the maps of the scalar and pseudo-scalar potentials ψ_E and ψ_B which are directly related to the electric and magnetic types of polarization, respectively. Their difference maps, shown in Figs 3 and 4, present distinct degree-scale distributions in the MS-modified-LP and unmodified-LP cases (where the latter is obtained from the unmodified LensPix code as previously explained), owing to the power transfer from non-linear to large scales in the lensed *E* and *B* fields.

As a quantitative study of the simulated maps, we have performed power spectrum and one-point statistics analyses. We find that the lensed TT, TE, EE and BB power spectra, obtained using the MS dark matter distribution, mostly overlap with the corresponding semi-analytic expectations on a range of multipoles up to $l \sim 2500$ (see Figs 6–8). This latter result points out the effectiveness of the MS in reproducing correctly the findings of the theoretical approach. Furthermore, an excess of power is observable in the MS-modified-LP case on larger multipoles, in particular for the *BB* spectrum. We believe that this excess originates from the accurate inclusion of non-linear power in the MS, which is present in the MS lensing potential power spectrum as well (Fig. 1). This outcome should be taken into account in the various delensing approaches, since these non-linear effects can have an impact on the quality of the reconstructed unlensed sky, particularly in view of the detection of primary B modes.

Finally, we have derived one-point statistics both of the simulated *T*, *Q*, *U* lensed maps and of the corresponding difference maps, in the MS-modified-LP and unmodified-LP cases. The comparison of the resulting PDFs with respect to Gaussian random distributions with the same mean and standard deviation does not show any statistical difference when the total lensed maps are considered. On the other hand, we find that the difference maps are characterized by a kurtosis excess. This result represents the distinctive weak-lensing effect of inducing non-Gaussianity in the unlensed Gaussian CMB field. This is simply explained if in first approximation we think of the lensed field as the product of two Gaussian fields, i.e. the lensing potential and the primary unlensed CMB. Actually, correctly speaking, the lensing potential map, derived by integration of the MS dark matter distribution, preserves an intrinsic degree of non-Gaussianity due to the non-linear evolution of the cosmic structures, which at some level contributes to the non-Gaussian statistics of the simulated lensed CMB. Unfortunately, the one-point statistic is not sufficient to disentangle the two contributions, i.e. the dominant effect coming from the product of two different fields, and the subdominant effect coming from the non-linear matter evolution. This is the reason why in Fig. 11 there seems to be no difference between the MS-modified-LP and unmodified-LP cases. We reserve a more accurate characterization of non-Gaussianity in CMB lensing statistics to a future work.

Downloaded from http://mnras.oxfordjournals.org/ at INAF Brera Milano (Osservatorio Astronomico di Brera) on January 9, 2015

ACKNOWLEDGMENTS

CC warmly thanks L. Verde for precious suggestions, and E. Gaztanaga, P. Fosalba, S. Leach and M. Liguori for helpful discussions. CB thanks B. Menard for helpful suggestions. Some of the results in this paper have been derived using the Hierarchical Equal Area Latitude Pixelization of the sphere (Gorski et al. 2005). CC is supported through a Beatriu de Pinos grant.

REFERENCES

Acquaviva V., Baccigalupi C., 2006, Phys. Rev. D, 74, 103510
Afshordi N., 2004, Phys. Rev. D, 70, 083536
Amblard A., Vale C., White M., 2004, New Astron., 9, 687
Bartelmann M., Schneider P., 2001, Phys. Rep., 340, 291
Bunn E. F., Zaldarriaga M., Tegmark M., De Oliveira-Costa A., 2003, Phys. Rev. D, 67, 023501
Cabella P., Kamionkowski M., 2005, preprint (arXiv:astro-ph/0403392v2)
Carbone C., Springel V., Baccigalupi C., Bartelmann M., Matarrese S., 2008, MNRAS, 388, 1618
Challinor A., Chon G., 2002, Phys. Rev. D, 66, 127301
Challinor A., Lewis A., 2005, Phys. Rev. D, 71, 103010
Das S., Bode P., 2008, ApJ, 682, 1
Fosalba P., Gaztanaga E., Castander F., Manera M., 2008, MNRAS, 391, 435
Gorski K. M., Hivon E., Banday A. J., Wandelt B. D., Hansen F. K., Reinecke M., Bartelman M., 2005, ApJ, 622, 759
Hamimeche S., Lewis A., 2008, Phys. Rev. D, 77, 103013
Hirata C. M., Seljak U., 2003, Phys. Rev. D, 68, 083002
Hirata C. M., Ho S., Padmanabhan N., Seljak U., Bahcall N., 2008, Phys. Rev. D, 78, 043520
Hu W., 2000, Phys. Rev. D, 62, 043007-1
Hu W., Dodelson S., 2002, ARA&A, 40, 171
Hu W., Seljak U., White M., Zaldarriaga M., 1998, Phys. Rev. D, 57, 3290
Hu W., Huterer D., Smith K. M., 2006, ApJ, 650, L13
Kamionkowski M., Kosowsky A., 1999, Ann. Rev. Nucl. Part. Sci., 49, 77
Kamionkowski M., Kosowsky A., Stebbins A., 1997, Phys. Rev. D, 55, 7368.
Kesden M., Cooray A., Kamionkowski M., 2002, Phys. Rev. D, 66, 083007
Komatsu E. et al., 2009, ApJS, 180, 330
Lewis A., 2005, Phys. Rev. D, 71, 083008
Lewis A., Challinor A., 2006, Phys. Rep., 429, 1
Ma C. P., Bertschinger E., 1995, ApJ, 455, 7
Newman E. T., Penrose R., 1966, J. Math. Phys., 7, 863
Okamoto T., Hu W., 2002, Phys. Rev. D, 66, 063008
Pritchard J., Kamionkowski M., 2005, Annals. Phys., 318, 2
Refregier A., 2003, ARA&A, 41, 645
Reichardt C. L. et al., 2009, ApJ, 694, 1200
Seljak U., Hirata C. M., 2004, Phys. Rev. D, 69, 043005
Seljak U., Zaldarriaga M., 1997, Phys. Rev. Lett., 78, 2054
Smith R. E. et al., The Virgo Consortium, 2003, MNRAS, 341, 1311
Smith S., Challinor A., Rocha G., 2006a, Phys. Rev. D, 73, 023517
Smith K. M., Hu W., Kaplinghat M., 2006b, Phys. Rev. D, 74, 123002
Smith K. M., Zahn O., Dore O., 2007, Phys. Rev. D, 76, 043510
Spergel D. N. et al., 2003, ApJS, 148, 175
Springel V., Frenk C. S., White S. D. M., 2006, Nat, 1137, 440
Teyssier R. et al., 2008, A&A, preprint (doi:10.1051/0004-6361/200810657)
Zaldarriaga M., Seljak U., 1997, Phys. Rev. D, 55, 1830.
Zaldarriaga M., Seljak U., 1998, Phys. Rev. D, 58, 023003

This paper has been typeset from a TEX/LATEX file prepared by the author.

Downloaded from http://mnras.oxfordjournals.org/ at INAF Brera Milano (Osservatorio Astronomico di Brera) on January 9, 2015